AAS 14-431

UTILIZATION OF UNCERTAINTY INFORMATION IN ANGLES-ONLY INITIAL ORBIT DETERMINATION

Christopher R. Binz* **and Liam M. Healy***

In an initial orbit determination (IOD) problem with known sensor uncertainty characteristics, probabilistic information beyond the typical point solution may be derived. In previous work (AAS 13-822), the authors demonstrated methods of determining state uncertainty estimates directly from an angles-only IOD process. This paper extends the previous work by applying it to other IOD methods using angles-only observations, as well as simulating different orbits and observation geometries, including simultaneous measurements from multiple geographically-distinct ground sites. We also explore performance for using the IOD state and uncertainty estimate as a starting point when processing additional observations.

INTRODUCTION

In the increasingly congested space environment,[1] accurate knowledge of the orbits of resident space objects is crucial. In order for this information to be of practical use, however, a quantitative estimate of the uncertainty of the state is also important. An accurate characterization of uncertainty can aid in such tasks as more accurate collision probability calculations and faster sensor acquisition. This work focuses on quantifying uncertainty in the problem of initial orbit determination (IOD) with angles measurements. In a typical orbit determination processing scheme, the estimate from the IOD algorithm is used as an initial seed to a batch least squares estimation process, which fits the orbit to a larger number of measurements, resulting in both a more refined orbit and the first expression of the uncertainty in the estimate.[2] Upon the collection of more measurements, the orbit can be refined with the usual methods (e.g. batch least squares, Kalman filtering). Typically, the uncertainty estimate from least squares is required to initialize a sequential estimation scheme. A covariance estimate directly from an IOD process could also aid in the problem of associating observations with catalogued objects, particularly with the covariance-based track association method.[3]

In a previous paper,[4] the basic approach to handling uncertainty in angles-only IOD was discussed. That work focused on Gauss's IOD method, and demonstrated how measurements with a uniform probability density transformed into state space. For a single low-Earth orbit example, the solution space was first found using Monte Carlo methods, then was estimated using the traditional least squares approach and a novel "sigma points" method (which will be discussed further later in this paper). For this example problem, it was shown that while the point solution was not significantly affected by the choice of technique, the uncertainty characterization from the sigma points method was significantly improved over that of the least squares technique (when compared with the "true" distribution from the Monte Carlo population). In this work, we demonstrate this across

*Mathematics and Orbit Dynamics Section, Naval Research Laboratory, Code 8233, 4555 Overlook Ave., SW, Washington, DC 20375-5355.

a much larger set of orbits, as well as explore other possible applications of realistic uncertainty estimates.

This problem has been examined by several others. Weisman, Majji, and Alfriend took an analytical approach and used the transformation of variables technique to map the probability density function (PDF) in the measurement domain to the orbit domain.[5] They showed that their technique is viable for automated filter initialization. DeMars and Jah used a probabilistic interpretation of the admissible region—a bounded domain in range/range rate space—to represent the uncertainty in the solution.[6] They also show the ability of their method to consistently initialize and track an object in orbit.

Part of the motivation behind this work, as well as the reason for choosing to model ground sensors with a uniform probability density over the field of view (i.e. *binary sensors*) stems from the idea of *Ubiquitous Low-Cost Sensors* (ULCS).[7] This shifts the paradigm of high-quality observations obtained from a few high-quality (and high-cost) sensors towards a larger number of inexpensive sensors that are widely deployed, but perhaps significantly noisier. With careful handling of the probabilistic elements involved, some surveillance requirements may be met with these sensors, thus allowing for much greater coverage than is feasible with expensive and/or legacy systems.

METHODOLOGY

This paper continues to use Gauss's method for IOD,[8] although the processes should be applicable to any. Like the previous paper, measurements are assumed to be generated from a binary sensor—that is, a measurement is recorded when the satellite is detected anywhere within the instrument's field of view. This is modeled with a uniform probability density for each measurement over the sensor field of view, which is 0.5° in this work. This measurement uncertainty can be handled in multiple ways. For a general least squares process, it may be specified as a measurement covariance matrix, and used in the calculation. Alternatively, the concept of sigma points may be adapted from the unscented transform, a process which is described below.

Sigma Points

Following Julier,[9] a set of deterministically-chosen, weighted points from each measurement distribution may be constructed such that the first two statistical moments of the true distribution are preserved. The process for constructing this set is discussed in the authors' previous paper.[4] The required number of points for a two-dimensional distribution is $2 \cdot 2 + 1 = 5$. Doing this for each measurement results in three sets of five measurement sigma points. Taking every possible combination of three measurements, the IOD is performed $5 \cdot 5 \cdot 5 = 125$ times, resulting in a solution space population consisting of 125 samples. This process is outlined in Figure 2.

In some cases, the observation geometry is such that the resulting IOD sample is unrealistic: orbits which intersect the Earth, hyperbolic orbits, etc. Unrealistic samples may be screened simply by checking to make sure they pass a few basic tests. For this work, the constraints were on eccentricity e and semimajor axis a:

$$0 \leq e < 1 \tag{1}$$

$$6378 \leq a \leq 40000 \tag{2}$$

Essentially all sigma points which are not closed Earth orbits with a semimajor axis greater than the radius of Earth and less than some large upper bound are rejected. Once a sample is rejected, the

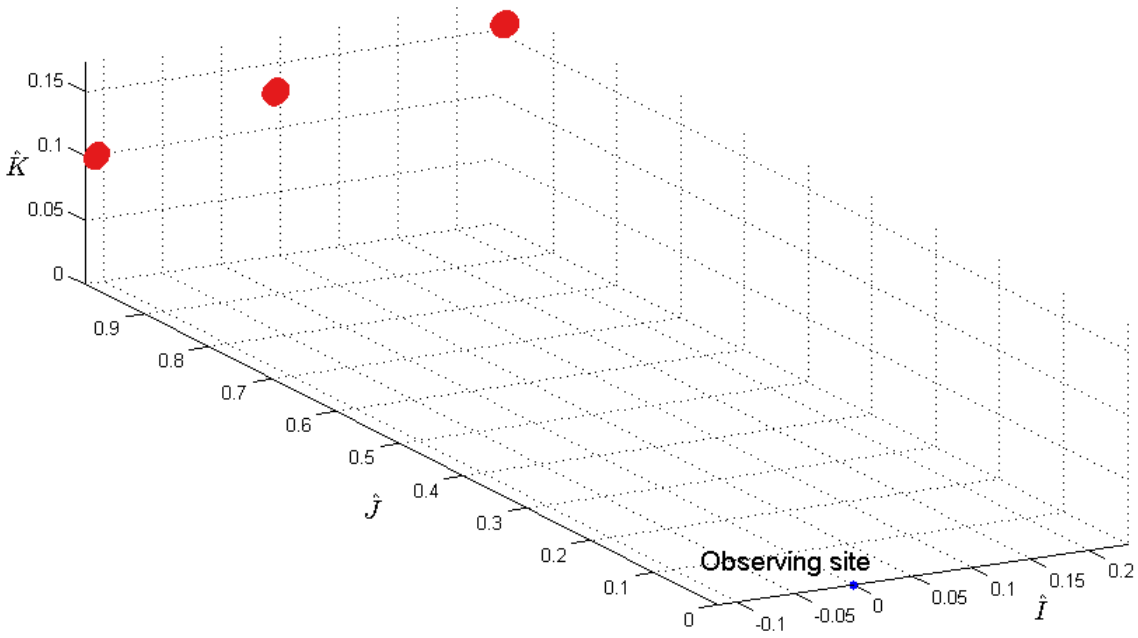

Figure 1. Example set of observations (red) from a ground site (blue) in the topocentric frame. Measurements are unit vectors in the topocentric frame.

entire set of sigma point solutions needs to be reweighted. Given the original set of weights for the mean and covariance W_m and W_c, the updated weights W'_m and W'_c are given by

$$W_m'^{(i)} = \frac{W_m'^{(i)}}{\sum_i W_m'^{(i)}} \tag{3}$$

$$W_c'^{(i)} = \frac{W_c'^{(i)}}{\sum_i W_c'^{(i)}} \tag{4}$$

This process renormalizes the weights and ensures the relative contributions of all samples to the final ensemble is preserved.

Once the screening is complete, the remaining population of orbit samples may be used to construct the mean and covariance of the estimate. Given the solutions $\boldsymbol{y}^{(i)}$ and the augmented weighting vectors W'_m and W'_c, the mean $\boldsymbol{m}$ and covariance $\boldsymbol{P}$ of the sample set is:

$$\boldsymbol{m} \approx \sum_{i=0}^{m} W_m'^{(i)} \boldsymbol{y}^{(i)} \tag{5}$$

$$\boldsymbol{P} \approx \sum_{i=0}^{m} W_c'^{(i)} (\boldsymbol{y}^{(i)} - \boldsymbol{m})(\boldsymbol{y}^{(i)} - \boldsymbol{m})^T \tag{6}$$

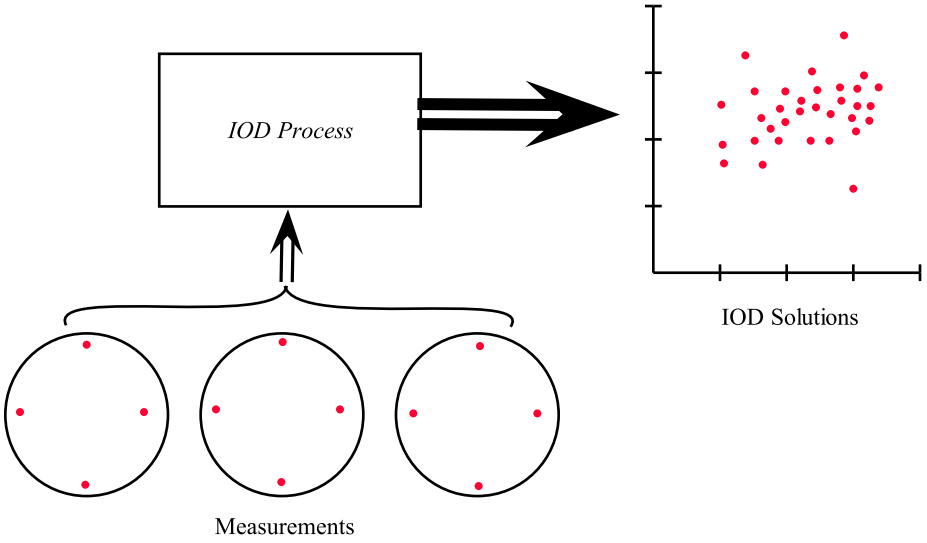

Figure 2. Overall process for describing IOD solution-space distribution with sigma points.

Simulation

Simulated observations are generated according to the following process. First, the true orbit is propagated, and angles (specifically topocentric right ascension and declination) are recorded for ground station passes. In this work, the time between observations is 150 seconds. These observations are then corrupted with uniform noise across the simulated field of view of the optical sensor, such that the true observation does not lie at the center of the simulated field of view. A consecutive set of three corrupted observations are chosen, and the IOD process is performed. In addition to uncertainty characteristics of the resulting estimates, the *error* itself may be found, since the "truth" is simulated and known. A basic two-body orbit propagator is used in this work.

A set of random orbits is generated from Keplerian elements drawn from a uniform probability distribution function. A simple acceptance test is performed to make sure the combination of the eccentricity and semimajor axis does not result in a perigee which is lower than the radius of the Earth. The bounding values for each element are listed in Table 1. Each is propagated, and those which pass over the given ground station long enough to produce a set of at least three measurements is used in the analysis. In this way, the performance of the algorithms may be tested on a large number of orbit geometries. The notional ground site is located at 30° N, 80° W, and the field of regard of the sensor is the entire sky with a 5° elevation mask.

Additionally, note that because of the way the sampling is done, the actual number of orbits which produce observations is not deterministic, and so the number of samples the user requests is only an upper limit. In other words, while the user specifies the number of orbits to simulate, the total number of orbits that produce the requisite number of observations over the given ground station may be less. For a more rigorous probabilistic treatment of orbits, refer to Healy and Binz.[10]

This paper presents several scenarios. First, the analysis of the previous paper—IOD from a single ground station—is repeated with a larger sample size. Second, a scenario in which there are two geographically-distinct observing sites, gathering measurements on the same object, is presented. The IOD process is performed at both sites, then combined. The fusion of these two estimates

Table 1. Range of Keplerian elements used for sampling.

a [km]	7000–9000
e	1×10^{-5}–0.1
i [deg.]	0–180
Ω [deg.]	0–360
ω [deg.]	0–360
ν [deg.]	0–360

assumes that they are independent, and is done according to the process in Tapley, Schutz, and Born:[11]

$$\boldsymbol{m} = (\boldsymbol{P}_1^{-1} + \boldsymbol{P}_2^{-1})^{-1}(\boldsymbol{P}_1^{-1}\boldsymbol{m}_1 + \boldsymbol{P}_2^{-1}\boldsymbol{m}_2)^{-1} \tag{7}$$

$$\boldsymbol{P} = (\boldsymbol{P}_1^{-1} + \boldsymbol{P}_2^{-1})^{-1} \tag{8}$$

Effectively, this is the intersection of two different distributions in solution space, exploiting the different geometries from two distinct observing sites.

Finally, estimation performance is examined for two representative cases (with varying sensor field of view) when the IOD state and covariance estimate is used to initialize a processing scheme for more than three measurements. For a single pass that produces at least 10 measurements, the first three are used in the sigma point IOD process, and the resulting solution is refined using an unscented Kalman filter (UKF) to process the remaining measurements.

RESULTS

As in the first paper, the solution space is examined in modified equinoctial elements as defined by Walker, Ireland, and Owens:[12] (p, f, g, h, k, L):

$$\begin{aligned} &p \text{ – semilatus rectum} && L = \omega + I\Omega + \nu \\ &f = e\cos(\omega + \Omega) && g = e\sin(\omega + \Omega) \\ &h = \tan^I\frac{i}{2}\cos\Omega && k = \tan^I\frac{i}{2}\sin\Omega \end{aligned} \tag{9}$$

Here, I is the "retrograde factor":[13] $+1$ for posigrade orbits and -1 for retrograde. There are two main reasons for using this element set. First, unlike the classical orbital element set, it is nonsingular for any eccentricity or inclination. Second, it is a more natural coordinate system for describing orbits than, for instance, Cartesian, in that only one coordinate changes in time for unperturbed motion (as with the classical set). Previous work has shown that uncertainty descriptions in equinoctial element space remain valid for a longer period of time than descriptions in Cartesian space,[14] which is a result of the fact that propagation in equinoctial coordinates is a nearly linear process for basic Keplerian motion (and can in fact be made linear through the use of mean motion n instead of semilatus rectum and mean anomaly instead of true longitude L).[15]

In assessing the performance of these methods, Mahalanobis distance is utilized. The Mahalanobis distance k of a sample $\boldsymbol{X}$ from the normal distribution $\mathcal{N}(\boldsymbol{\mu}, \boldsymbol{P})$ is defined as

$$k = \sqrt{(\boldsymbol{X} - \boldsymbol{\mu})\boldsymbol{P}^{-1}(\boldsymbol{X} - \boldsymbol{\mu})^{-1}} \tag{10}$$

In colloquial terms, k can be thought of as the "number of sigmas" away from the mean that the sample falls. Framed this way, we see that the distribution of the Mahalanobis distances of a large number of samples drawn from a normal distribution should follow a well-defined distribution itself—in fact, it takes the form of the χ distribution.[16]

In looking at the different orbit samples in aggregate, two aspects of the estimates are plotted. First, the error in each modified equinoctial element at the fit epoch is plotted. Then, the Mahalanobis distance of the *true orbit* from the *estimated mean and covariance* is calculated as a metric for how realistic the uncertainty from the fit is. It is important to note that while a low Mahalanobis distance is good in that it means the uncertainty estimate contains the truth, it may simply be the case that the uncertainty estimate is so large that even distant points are within some n-sigma range. Put another way, a low Mahalanobis distance does not necessarily correspond to a low absolute error. It may, however, aid in applications such as covariance-based track association.

In addition to uncertainty, we are able to measure *error* since we know the simulated truth. This metric is simply the difference in each coordinate—for a distribution, it is the difference of the mean from the truth—and does not consider probabilistic information. Loosely, the error gives the quality of the estimated *mean*, while something like the Mahalanobis distance gives the quality of the *uncertainty description*.

Single Site IOD

The error in each element is plotted in Figure 3. In addition to each sample being plotted as a point, the sample population mean for both methods is plotted as a horizontal line. In order to show detail at the lower end of the plots, they were resized such that some of the higher least squares results are not shown. In all coordinates, the sigma point method performs better than the least squares fit on average.

Figure 4 shows the Mahalanobis distance values of each truth orbit solution to its corresponding mean and covariance from each method. Again some very high values of k do not appear within the limits of this plot. On average, the Mahalanobis distance resulting from the sigma point method is low—usually from 1–4—suggesting a covariance that does a proper job of describing the true uncertainty in the fit.

Multiple Site IOD

For this analysis, a second site is placed at 30° N, 85° W (5° West of the first site), with the same field of regard as the first site (5°) elevation mask. The error for the two-site, fused estimates is plotted in Figure 5. Again, there is a marked improvement over the least squares technique with the sigma points, which in some coordinates is more pronounced than with the single-site case.

Figure 6 shows the sigma point uncertainty contributions from each site: the Mahalanobis distance of truth from each site's estimated mean and covariance. The geographic separation leads to a slightly different geometry, which results in differing estimates. The result of the fusion of the two estimates is plotted in Figure 7, along with the fused least squares estimates.

The trend of lower values of k from the sigma point method continues here. Figure 7 looks very similar to Figure 4, but the significantly lower error shows that the fused estimate from two sites is superior to that from a single site. It is also interesting to note that the mean Mahalanobis distance from the sigma point method of 2.11 is quite close to the expected mean of the χ distribution (2.35). The distribution of Mahalanobis distances for a normally-distributed random vector follows the χ

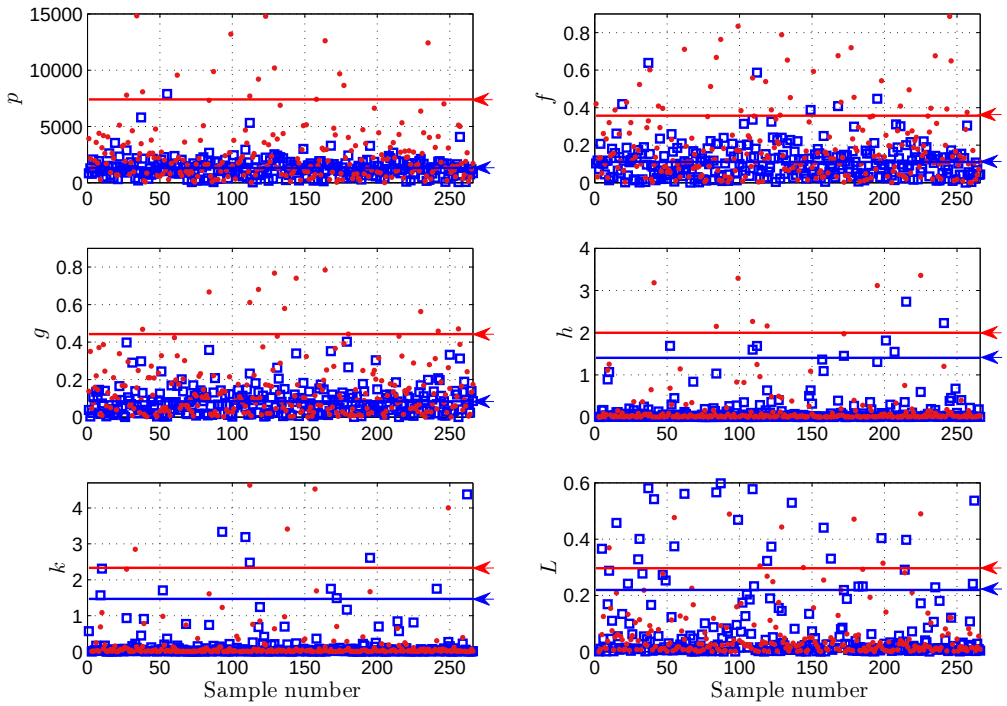

Figure 3. Error in single-site case. Blue points are from the sigma point method, red are from a least squares fit. Horizontal lines are mean values over the sample population.

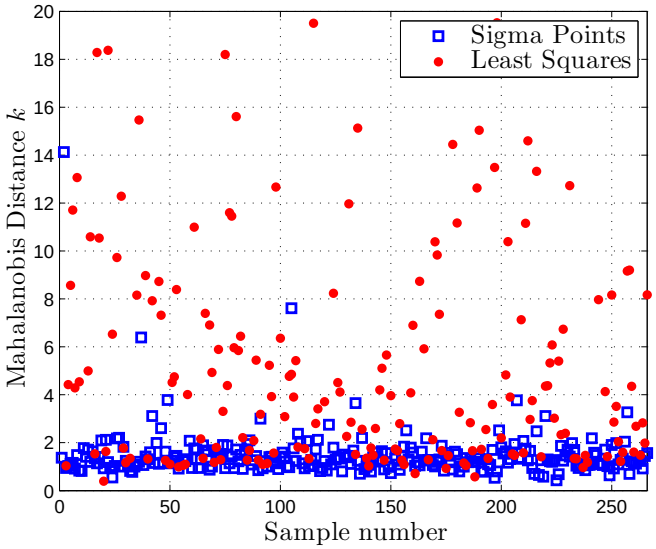

Figure 4. Mahalanobis distances for the single-site case. The mean value is 350.0 for least squares, and 1.48 for sigma points.

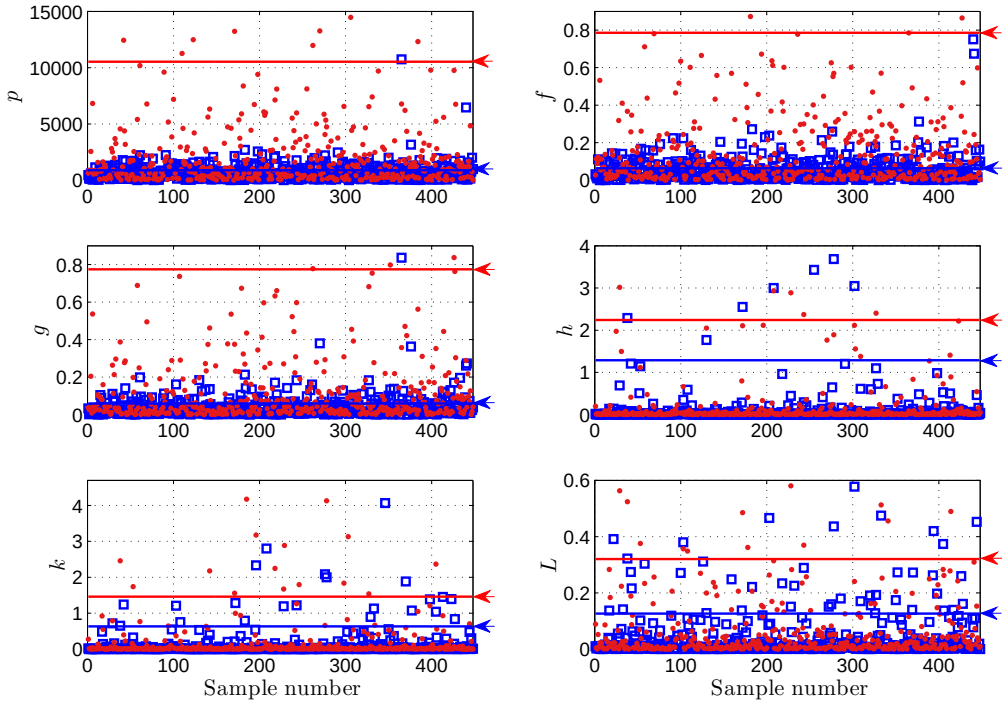

Figure 5. Error in two-site case. Blue points are from the sigma point method, red are from a least squares fit. Horizontal lines are mean values over the sample population.

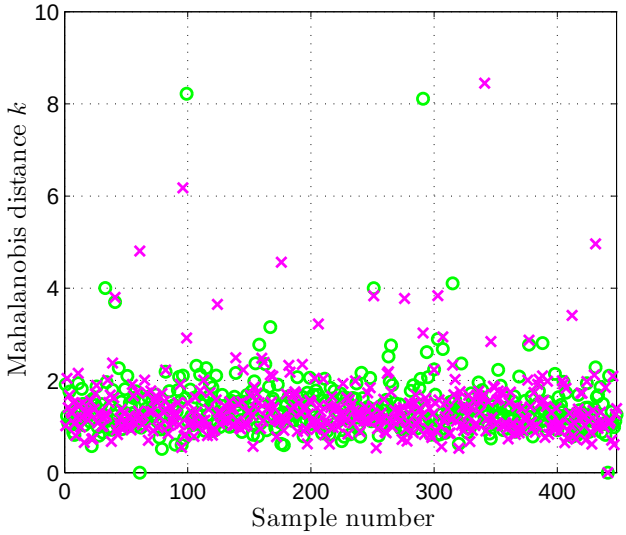

Figure 6. Mahalanobis distance for the sigma point estimates from each site.

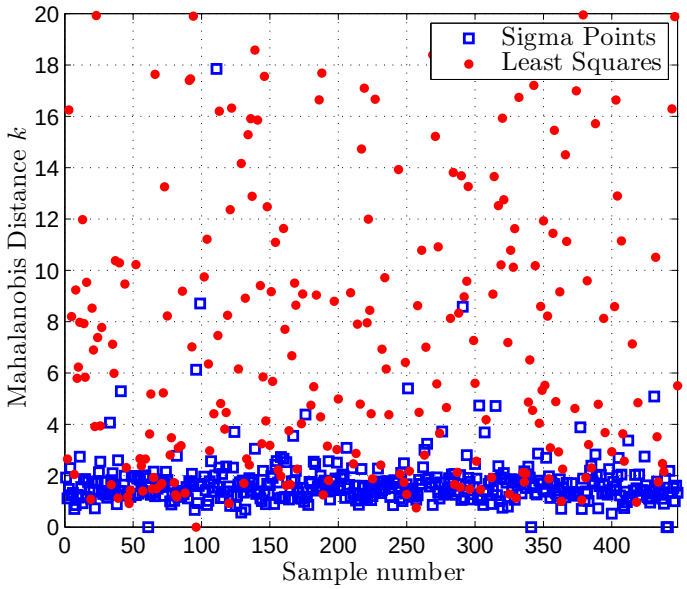

Figure 7. Mahalanobis distances from the fused estimates of both sites. The mean value is 52.4 for least squares, and 2.11 for sigma points.

Table 2. Average error over all sampled orbits.

Scenario		p [km]	f	g	h	k	L [rad]
Single site	Least Squares	7394.1	0.35753	0.44240	1.9976	2.3345	0.29633
	Sigma Points	1314.3	0.11022	0.084179	1.4051	1.4694	0.21939
Multiple sites	Least Squares	10528.	0.78560	0.77426	2.2404	1.4619	0.31992
	Sigma Points	881.14	0.063622	0.059326	1.2872	0.63462	0.12617

distribution,[16] therefore this indicates that the PDF resulting from the sigma point method represents the actual distribution quite well.

Table 2 presents the average error in each coordinate over all orbit samples. Note that the poor uncertainty description from the least squares process manifests in a *worse* estimate from multiple sites than with a single site, since the fused estimate is a combination of two unrealistic covariances.

Figure 8 shows one representative orbit sample with estimates from each site, along with the fused solutions. The error is diminished significantly in the fused estimates, as is the uncertainty. In particular, note that the variance in semilatus rectum p is much lower than either of the two single-site solutions—this is a direct result of the range being more observable with multiple ground sites.

Single Site Continued Estimation

For this scenario, the simulation was limited to producing orbits which passed over a single site long enough to produce at least 10 equally-spaced observations. The results of a single orbit sample are presented here. Figure 9 graphically depicts the uncertainty by randomly sampling the

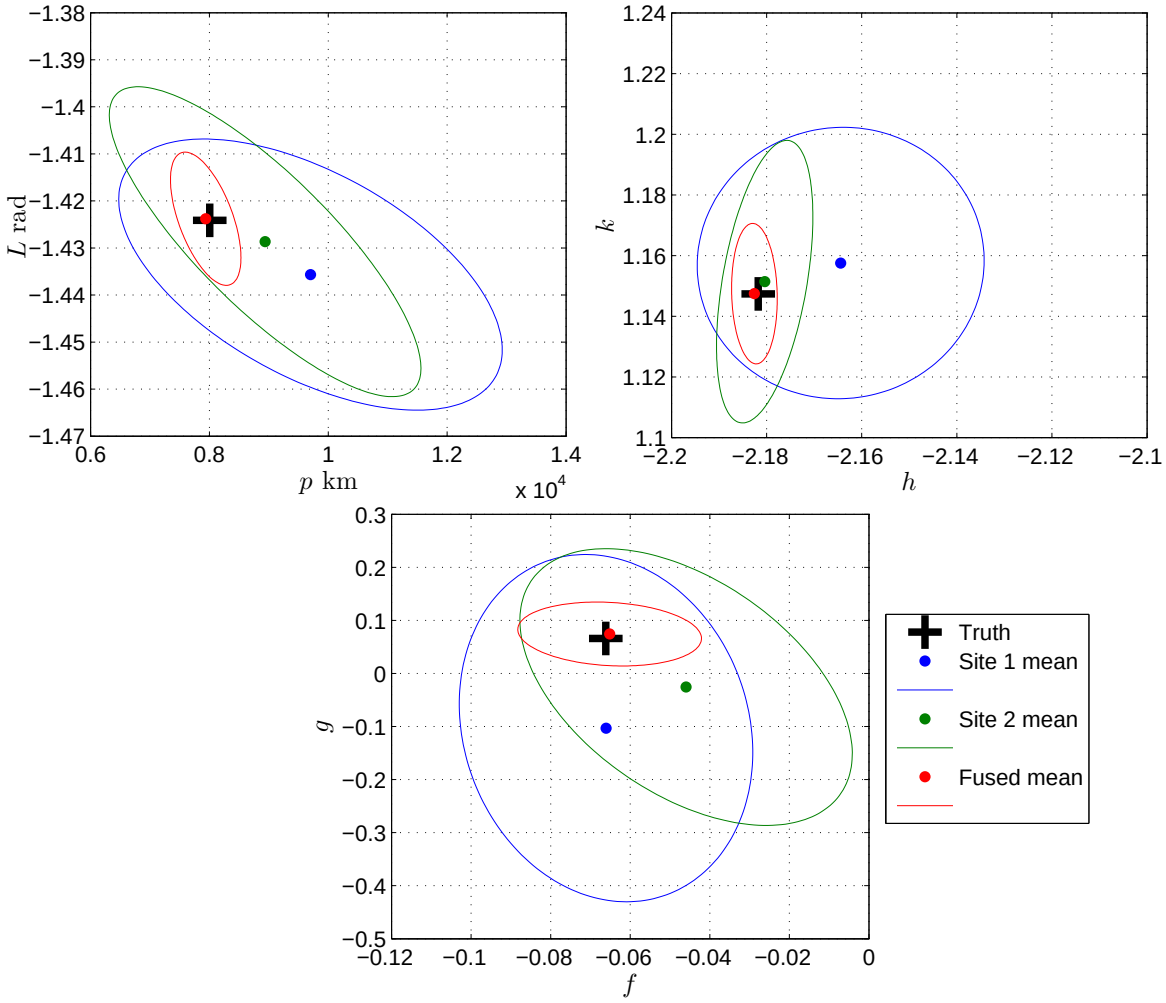

Figure 8. Fusion of estimates from different observing sites using the sigma point algorithm.

covariance of the estimate at each time step. Figure 10 shows how the error in each coordinate is affected by subsequent measurement processing.

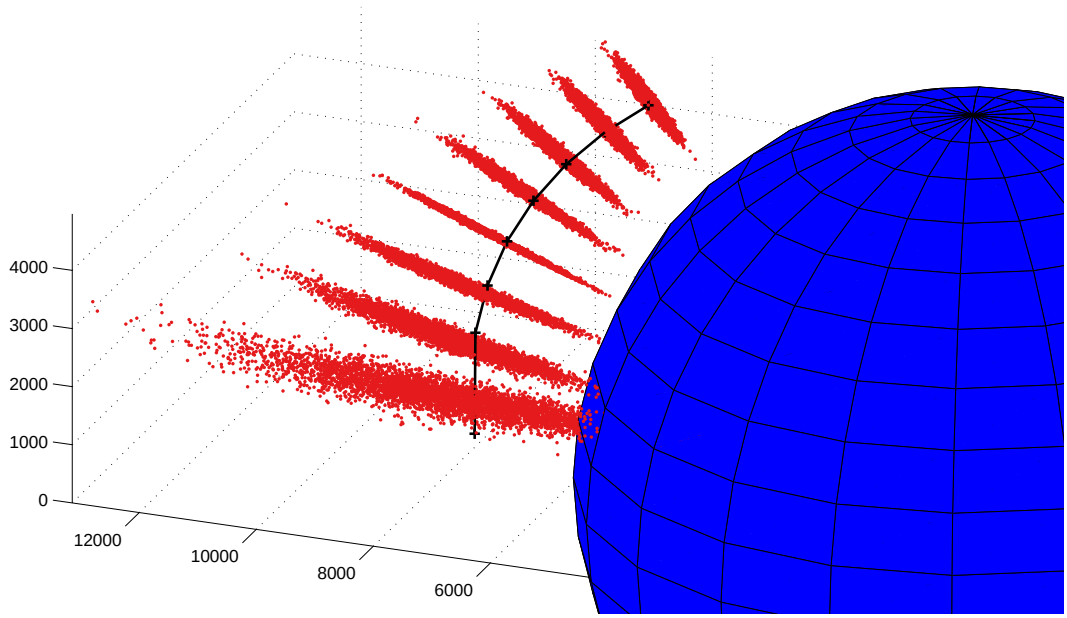

Figure 9. Graphical depiction of uncertainty evolution as more observations are processed. True orbit is plotted in black, red dots are sampled from the covariance at each step.

The bulk of the uncertainty lies in the coordinate corresponding to orbital energy—here, semilatus rectum. This is an intuitive result of an estimation scheme in which only angles are directly observable. Unfortunately, uncertainty in this coordinate is the largest contributor to growth in uncertainty in the "fast" angular variable (here, true longitude L).[15] In general, reducing this component of the uncertainty is difficult with angles-only measurements. In this particular example, the uncertainty in semilatus rectum results in a true longitude uncertainty of nearly 66° after a single orbit. However, the solution is significantly better in the other coordinates, and if a surveillance system could be made insensitive to in-track error, reacquisition could be feasible with such a solution.

Figures 11 and 12 show the results of another single-site estimation case with a smaller sensor field of view (FOV) of 0.05°. While this is an order of magnitude lower than the FOV used in the previous cases, it is still an order of magnitude larger than typical noise values for space surveillance telescopes.[17] As expected, these results are significantly better, particularly in semilatus rectum. However, the 10x reduction in sensor FOV does not quite yield a 10x reduction in error: the true longitude is off by just under 10° after a single orbit. Even so, the quality of the solution may be good enough to cue a downrange sensor or associate the track with a known, catalogued object.

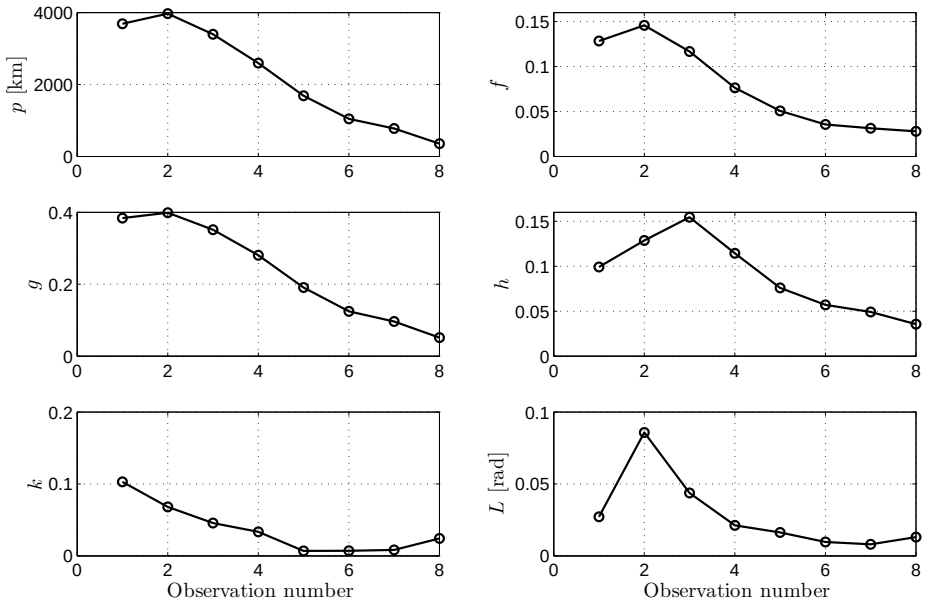

Figure 10. Error in the estimate at each observation time.

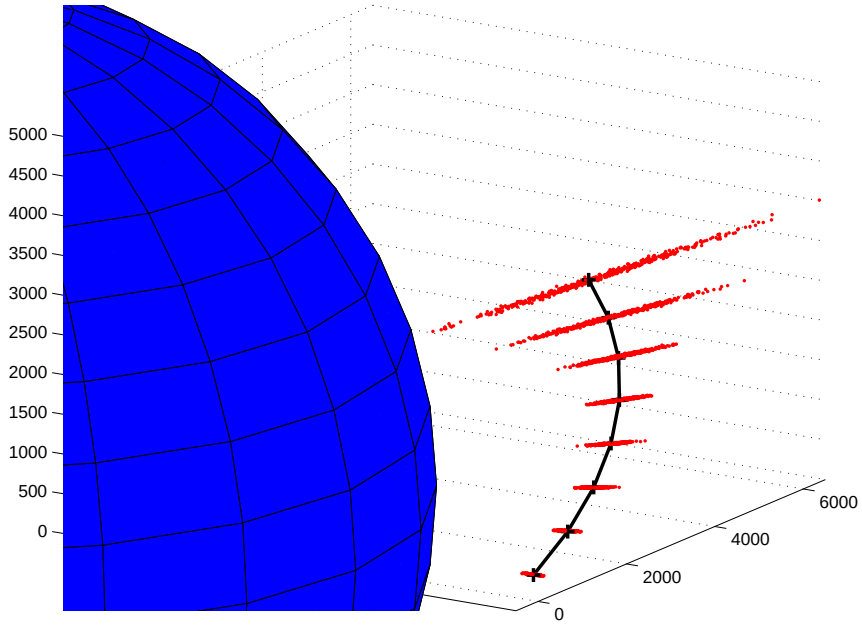

Figure 11. Sequential processing for a case with a smaller sensor FOV. True orbit is plotted in black, red dots are sampled from the covariance at each step.

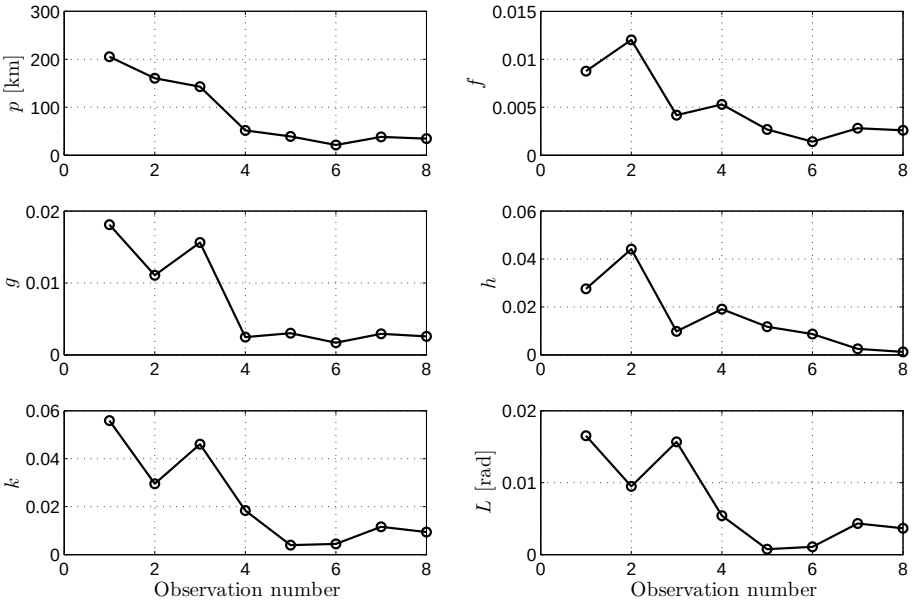

Figure 12. Error in the estimate at each observation time.

DISCUSSION

The first part of this paper quantified the performance of Gauss's IOD method for a range of low Earth orbits. As this method produces only a point solution, uncertainty estimates were obtained first with the more traditional weighted least squares technique, then with the adapted sigma points technique. While the performance of Gauss's method alone is not particularly good, the two techniques for obtaining an uncertainty estimate vary significantly. The least squares uncertainty estimate is a poor overall fit of the true distribution; it generally fails to capture the actual structure of the distribution, and typically provides an overly optimistic description.

The sigma point method does a much better job of describing the true nature of the uncertainty in the estimate, as evidenced by the consistently lower Mahalanobis distances from the simulated truth solution. Additionally, the ability to filter out particularly poor sigma points from the overall population allows for a consistently lower error in the mean of the estimate.

The benefits of a more accurate uncertainty description (evidenced by lower Mahalanobis distances) are perhaps most evident in an covariance-based observation association scheme. A more realistic covariance increases the likelihood that the track will be associated with the correct object. The fact that the technique presented here produces lower Mahalanobis distances than the least squares method even with the minimum set of three observations suggests that it may be beneficial to investigate further.

As the results show consistently large error in the semilatus rectum coordinate, any technique that reduces this is worthy of consideration. The second scenario presented here explored one such technique: fusing the orbit estimates from two geographically-distinct observing sites. This, in effect, gives a better direct estimate of range from the ground stations, which helps to reduce the

uncertainty in the in-plane orbit elements. As a result, the multiple-site estimation cases yielded significantly more accurate and precise orbit estimates, as expected.

The third scenario presented limited results for a single-pass estimation scheme from a single ground station. These situations do a good job of illustrating just how limited angles-only initial orbit determination really is. Promisingly, for the example cases shown, the filter used was able to converge properly, and further measurements were used to drive down uncertainty in the estimate. However, for the number of measurements used, the solution reaches only a limited level of accuracy—the semilatus rectum is still highly uncertain, which makes the problem of reacquiring the object after one or more orbit periods difficult.

The final case presented, with a smaller FOV, outlines an interesting inherent trade between sensor resolution or FOV and accuracy. Given a surveillance system architecture, one could derive tracking accuracy requirements, then map them back to a physical, sensor-level parameter. This method is preferred over simply choosing the most accurate sensor available, as there may be significant cost savings in choosing a slightly less capable sensor. As an example, while the solutions shown here may not be precise enough to add the object to the catalog, they may be sufficient to cue a downrange sensor or, as previously discussed, associate the observations with a known object.

FUTURE WORK

For the purposes of this paper, sampling was limited to changing the orbit parameters. However, there are many parameters in this problem that affect performance, including different measurement uncertainty values and measurement frequency. While the measurement frequency was explored in the initial stages of this work, investigating different values may improve aspects of this work.

Measurement noise/uncertainty is obviously a direct influence on the accuracy of the solutions, and it may be interesting to depart from the assumption of low-cost, low-quality sensors and see what is possible with measurements that are representative of most contemporary space surveillance sensors. Related to this is the choice of probability density function to represent the measurement: modeling a more realistic Gaussian distribution could make this work more directly applicable to current space surveillance problems.

The sigma point method described here and in the previous paper is applicable to any angles-only initial orbit determination method, of which there are several. Of course, there is nothing inherent in this technique that excludes the use of measurements of quantities other than angles, such as range or range rate. It may be an interesting exercise to observe how much this technique improves the initial uncertainty estimate for any IOD process, particularly after seeing how poorly a least-squares fit may describe the actual initial uncertainty in a measurement-lean environment.

REFERENCES

[1] "Satellite Box Score," *Orbital Debris Quarterly News* (J. Liu, ed.), Vol. 17, 2013.

[2] J. Sharma, G. H. Stokes, C. v. Braun, G. Zollinger, and A. J. Wiseman, "Toward operational space-based space surveillance," *Lincoln Laboratory Journal*, Vol. 13, No. 2, 2002, pp. 309–334.

[3] K. Hill, K. T. Alfriend, and C. Sabol, "Covariance-based uncorrelated track association," *AIAA/AAS Astrodynamics Specialist Conference and Exhibit*, AIAA/AAS, AIAA, 2008, doi:10.2514/6.2008-7211.

[4] C. Binz and L. Healy, "Uncertainty characterization for angles-only initial orbit determination," *Astrodynamics 2013*, Advances in the Astronautical Sciences, San Diego, CA, Univelt, Inc., 2013. AAS 13-822.

[5] R. M. Weisman, M. Majji, and K. T. Alfriend, "Analytic characterization of measurement uncertainty and initial orbit determination orbital element uncertainty and correlation," *Spaceflight Mechanics 2013*,

Vol. 148 of *Advances in the Astronautical Sciences*, San Diego, CA, AAS, Univelt, Inc., 2013. AAS 13-203.

[6] K. J. DeMars and M. K. Jah, "Probabilistic Initial Orbit Determination Using Gaussian Mixture Models," *Journal of Guidance, Control, and Dynamics*, Vol. 36, No. 5, 2013, pp. 1324–1335.

[7] L. Healy and C. Binz, "Measurement uncertainty in satellite direction finding with an interferometer," *Spaceflight Mechanics 2013*, Vol. 148 of *Advances in the Astronautical Sciences*, San Diego, CA, Univelt, Inc., 2013. AAS 13-276.

[8] A. C. Long, J. O. Capellari, Jr., C. E. Velez, and A. J. Fuchs, "Goddard trajectory determination system (GTDS) mathematical theory, Revision 1," tech. rep., NASA Goddard Space Flight Center, 1989.

[9] S. J. Julier and J. K. Uhlmann, "Unscented filtering and nonlinear estimation," *Proceedings of the IEEE*, Vol. 92, 2004, pp. 401–422.

[10] L. M. Healy and C. R. Binz, "Orbital density determination from unassociated observations: uninformative prior and initial observation," *Space Flight Mechanics 2014*, Vol. 151 of *Advances in the Astronautical Sciences*, San Diego, CA, AAS, Univelt, Inc., 2014. AAS 14-347.

[11] B. D. Tapley, B. E. Schutz, and G. H. Born, *Statistical Orbit Determination*. Burlington, MA: Elsevier Academic Press, 2004.

[12] M. Walker, B. Ireland, and J. Owens, "A set of modified equinoctial orbit elements," *Celestial Mechanics*, Vol. 36, No. 4, 1985, pp. 409–419. doi:10.1007/BF01227493.

[13] G. R. Hintz, "Survey of orbit element sets," *Journal of Guidance, Control, and Dynamics*, Vol. 31, No. 3, 2008, pp. 785–790.

[14] C. Sabol, T. Sukut, K. Hill, K. T. Alfriend, B. Wright, Y. Li, and P. Schumacher, "Linearized orbit covariance generation and propagation analysis via simple Monte Carlo simulations," *Spaceflight Mechanics 2010*, Vol. 136 of *Advances in the Astronautical Sciences*, San Diego, CA, Univelt, Inc., 2010. AAS 10-134.

[15] J. T. Horwood, N. D. Aragon, and A. B. Poore, "Gaussian Sum Filters for Space Surveillance: Theory and Simulations," *Journal of Guidance, Control, and Dynamics*, Vol. 34, November–December 2011, pp. 1839–1851.

[16] S. Blackman and R. Popoli, *Design and Analysis of Modern Tracking Systems*. Norwood, MA: Artech House, Inc., 1st ed., 1999.

[17] D. A. Vallado, *Fundamentals of Astrodynamics and Applications*. Hawthorne, CA: Microcosm Press, 3rd ed., 2007.